

The Journal of Neuroscience

<https://jneurosci.msubmit.net>

JN-RM-2092-18R2

The lactate receptor HCAR1 modulates neuronal network activity through the activation of G α and G $\beta\gamma$ subunits

Jean-Yves Chatton, University of Lausanne

Haissa de Castro Abrantes, University of Lausanne

Marc Briquet, University of Lausanne

Céline Schmuziger, University of Lausanne

Leonardo Restivo, University of Lausanne

Julien Puyal, University of Lausanne

Nadia Rosenberg, University of Lausanne

Anne Rocher, University of Lausanne

Stefan Offermanns, Max-Planck-Institute for Heart and Lung Research

Commercial Interest:

The lactate receptor HCAR1 modulates neuronal network activity through the activation of G_{α} and $G_{\beta\gamma}$ subunits

by

Haïssa de Castro Abrantes¹, Marc Briquet¹, Céline Schmuziger¹, Leonardo Restivo¹, Julien Puyal¹, Nadia Rosenberg¹, Anne-Bérengère Rocher¹, Stefan Offermanns² and Jean-Yves Chatton^{1,3*}

¹ Department of Fundamental Neuroscience, University of Lausanne, 1005, Lausanne, Switzerland

² Department of Pharmacology, Max-Planck-Institute for Heart and Lung Research, Bad Nauheim, Germany

³ Cellular Imaging Facility, University of Lausanne, 1005, Lausanne, Switzerland

*Corresponding author:

Jean-Yves Chatton, PhD
Department of Fundamental Neuroscience
University of Lausanne
Rue Bugnon 9
CH-1005 Lausanne, Switzerland
Tel. +41-21-692-5106 // Fax: +41-21-692-5105 // e-mail: jean-yves.chatton@unil.ch

Content: Number of pages: 41
Number of tables: 6
Number of figures: 6
Number of words for abstract: 237
Number of words for introduction: 556
Number of words for discussion: 1482

Abbreviated title: HCAR1 and neuronal activity

Conflict of interest: The authors declare no competing financial interests

Acknowledgments: This work was supported by the Swiss National Science Foundation (grant# 31003A_179399). The Epac2-camps plasmid was kindly provided by Jean-Pierre Hornung (University of Lausanne, Switzerland). We thank Joel Wellbourne-Wood for his critical reading of the manuscript and Christiane Devenoges for the genotyping.

1 Abstract

2 The discovery of a G protein-coupled receptor for lactate named hydroxycarboxylic acid receptor 1 (HCAR1) in
3 neurons has pointed to additional non-metabolic effects of lactate for regulating neuronal network activity. In
4 this study, we characterized the intracellular pathways engaged by HCAR1 activation, using mouse primary
5 cortical neurons from wild-type (WT) and HCAR1 knock-out (KO) mice from both sexes. Using whole-cell patch-
6 clamp, we found that activation of HCAR1 with 3-chloro-5-hydroxybenzoic acid (3Cl-HBA) decreased miniature
7 excitatory postsynaptic current frequency, increased paired-pulse ratio, decreased firing frequency, and
8 modulated membrane intrinsic properties. Using fast calcium imaging, we show that HCAR1 agonists, 3,5-
9 dihydroxybenzoic acid (3,5-DHBA), 3Cl-HBA, and lactate decreased by 40% spontaneous calcium spiking
10 activity of primary cortical neurons from WT but not from HCAR1 KO mice. Notably, in neurons lacking HCAR1
11 the basal activity was increased compared to WT. HCAR1 mediates its effect in neurons through a $G_{i\alpha}$ -protein.
12 We observed that the adenylyl cyclase-cAMP-protein kinase A axis is involved in HCAR1 down-modulation of
13 neuronal activity. We found that HCAR1 interacts with adenosine A1, GABA_B, and α_2 -adrenergic receptors,
14 through a mechanism involving both its $G_{i\alpha}$ and $G_{i\beta\gamma}$ subunits, resulting in a complex modulation of neuronal
15 network activity. We conclude that HCAR1 activation in neurons causes a down-modulation of neuronal
16 activity through presynaptic mechanisms and by reducing neuronal excitability. HCAR1 activation engages both
17 $G_{i\alpha}$ and $G_{i\beta\gamma}$ intracellular pathways to functionally interact with other G_i -coupled receptors for the fine tuning
18 of neuronal activity.

19

20

21 Significance Statement

22

23 Expression of the lactate receptor HCAR1 was recently described in neurons. Here, we describe the
24 physiological role of this G-coupled receptor (GPCR) and its activation in neurons, providing information on its
25 expression and mechanism of action. We dissected out the intracellular pathway through which HCA1R
26 activation tunes down neuronal network activity. For the first time, we provide evidence for the functional
27 cross-talk of HCA1R with other GPCRs, such as GABA_B, adenosine A1 and α_{2A} adrenergic receptors. These
28 results set HCAR1 as a new player for the regulation of neuronal network activity acting in concert with other
29 established receptors. Thus, HCAR1 represents a novel therapeutic target for pathologies characterized by
30 network hyperexcitability dysfunction, such as epilepsy.

31

32 Introduction

33 Lactate has long been considered a waste product of cellular metabolism. In the central nervous system (CNS),
34 this concept was challenged in the 90s when lactate was proposed to play an important role as energy
35 substrate for neurons (Pellerin and Magistretti, 1994). Since then, several studies indicated the valuable
36 contribution of lactate as a metabolic fuel in several cell types, as a neuroprotective agent, as well as its role as
37 a signaling molecule (for reviews, see e.g. Gladden, 2004; Barros, 2013).

38 The extracellular level of lactate in the brain is estimated to be in the low millimolar range at the resting
39 state (Abi-Saab et al., 2002). It has also been reported that physical exercise increases L-lactate plasma levels
40 up to 10-20mM (Offermanns, 2017). Under these conditions the brain becomes a net consumer of lactate
41 (Dalsgaard et al., 2004). Upon synaptic activity lactate level undergoes a two-fold increase (Dienel et al., 2007).
42 The main cell type locally producing lactate in the brain is likely to be astrocytes, as recently reported in the *in*
43 *vivo* mouse brain (Mächler et al., 2016), although this notion was recently challenged (Diaz-Garcia et al., 2017).
44 The recent discovery of a new mechanism for lactate release from astrocytes through a K⁺-sensitive channel
45 (Sotelo-Hitschfeld et al., 2015), indicates that lactate can be rapidly mobilized and may possibly lead to a
46 transient elevation of its extracellular concentration to high levels in microdomains close to neuronal
47 membranes, including synapses.

48 Recent studies indicated that energy substrates and metabolites of the energy metabolism had
49 extracellular signaling properties by acting through the activation of G protein-coupled receptors (GPCRs) (Blad
50 et al., 2012; Husted et al., 2017). One of them, originally named GPR81, now known as hydroxycarboxylic acid
51 receptor 1 (HCAR1), has lactate as endogenous ligand (Cai et al., 2008). HCAR1 was initially described as being
52 markedly expressed in adipocytes, where its activation induces the inhibition of lipolysis through the activation
53 of a G_i-dependent intracellular pathway (Liu et al., 2009). Our research group was the first to demonstrate that
54 L-lactate and a HCAR1 agonist decreases spiking activity of cortical neurons in a pertussis-sensitive manner
55 (Bozzo et al., 2013). In the locus coeruleus, L-lactate had rather an excitatory effect suggesting the

56 involvement of a different receptor, possibly G_s-coupled, yet to be identified (Tang et al., 2014). The aim of the
57 present study was to explore the downstream effectors of HCAR1 activation and clarify the mechanisms
58 through which this receptor modulates neuronal activity in mouse cortical neurons.

59 We focused on the investigation of the intracellular pathway mediated by the activation of G_i-coupled
60 receptors, which classically inhibits the adenylyl cyclase (AC) as a first phase of the intracellular cascade that
61 contributes to the decrease in neuronal activity (Seino and Shibasaki, 2005). To explore these aspects, we
62 compared the modulatory effects of HCAR1 activation on neuronal activity of primary neurons from both wild-
63 type (WT) and HCAR1 knock-out (KO) mice, using electrophysiological recordings and calcium imaging. Our
64 study indicates that HCAR1 activation engages the AC-cAMP-PKA pathway and has a presynaptic effect, which
65 is accompanied by a decrease in neuronal excitability. We further discovered that HCAR1 interacts with other
66 G_i-coupled receptors to fine-tune neuronal activity through a complex bimodal mechanism that involves the
67 G_{βγ} subunit and activation of phospholipase C (PLC). This interaction adds a higher level of complexity to the
68 functional outcome of HCAR1 activation.

69 **Material and Methods**

70 Ethics statement

71 All experimental procedures were carried out in accordance with the recommendations of the Swiss Ordinance
72 on Animal Experimentation, and were specifically approved for this study by the Veterinary Affairs of the
73 Canton Vaud, Switzerland (authorizations# 1288.6 and 1288.7).

74 Animals

75 HCAR1 KO and mRFP-HCAR1 mouse lines were obtained from Max-Planck-Institute for Heart and Lung
76 Research (Bad Nauheim, Germany). The generation and validation of these lines have been previously
77 described (Ahmed et al., 2010). The genotype of all animals used for the experiments, was confirmed using
78 polymerase chain reaction (PCR) analysis.

79 Behavioral analysis

80 The assessment of general behavior along with neurological and motor functions was performed in WT and
81 HCAR1 KO male mice (8 and 15 weeks). In a first phase, mice went through a basic neurological screening to
82 assess their general behavior/appearance, muscle tone, and motor function. Mice were placed in a
83 transparent Plexiglas box and observed for 5 minutes by an experimenter blind to the genotype of the animals.
84 Mice were checked for stereotyped behavior, convulsions, compulsive licking, self-destructive biting, and
85 retropulsion. Next, the grasping reflex was tested by suspending the mouse by the tail and giving Yes/No score
86 for hindpaw clasping over three consecutive trials. The grip strength was assessed by placing the animal on a
87 grid and by gently pulling its tail; the mean score of three trials per animal was used for analysis. In the second
88 phase, home cage behavior was monitored in Phenotyper cages (Noldus Information Technology, Leesburg,
89 VA, USA; RRID:SCR_004074)) that allow the automated scoring of parameters related to locomotion,
90 stereotypic behavior, feeding, and nesting. Briefly, mice were individually placed inside the Phenotyper cage
91 for one day with water and food ad-libitum. A shelter was placed in one corner of the cage for automated

92 scoring of nesting behavior. An infrared camera tracked the mouse movements throughout the 1-day session
93 allowing the monitoring of the above parameters. All the behavior data were collected and analyzed using the
94 EthoVision XT 14 software (Noldus Information Technology, RRID:SCR-000441).

95 Cell culture and transfection

96 Mouse primary cultures from cortical neurons were prepared from E17 embryos, both male and female, from
97 either WT, HCAR1 KO, or mRFP-HCAR1 C57bl/6N mouse lines. After removing the meninges, extracted cortices
98 were incubated in 2ml of HBSS with 10mg/ml Worthington Trypsin for 20 minutes at 37°C, and then
99 mechanically dissociated in Neurobasal (Invitrogen, Basel, Switzerland) culture medium supplemented with
100 10% FCS. Dissociated cells were filtered using a 40µm nylon mesh cell strainer and re-suspended in Neurobasal
101 culture medium complemented with 2% SM1 (Stemcell Technologies, Vancouver, Canada), 20mM GlutaMAX
102 (Invitrogen), and 0.02mM glutamate. Cells were plated at a density of 20,000 cells/cm² in 12mm and 20mm
103 diameter glass coverslips, coated with poly-D-lysine and laminin (Sigma-Aldrich, Buchs, Switzerland). Half of
104 the culture medium was exchanged every five days by a maturation medium composed of BrainPhys medium
105 (Stemcell Technologies) and 2% SM1. Cells were used at DIV 12-18.

106 Transfection with the plasmid carrying the cAMP Förster resonance energy transfer (FRET)-based
107 biosensor (Epac2-camps) (Nikolaev et al., 2004) was performed using Lipofectamine 2000 (Invitrogen) by
108 adding 3µg of DNA for 5-6 hours. Cells were transfected at DIV 10-12 and used 48h after transfection.

109 DNA extraction and PCR

110 Tissue was collected from phalanges of WT and HCAR1 KO E17 embryos used for the primary culture
111 preparation. The tissue was incubated in the digestion buffer (in mM): NaCl 100, Tris 10, EDTA 25, 0.5% SDS
112 and 5% Proteinase K (Roche), for 2h at 57°C. After 3 steps of centrifugation, the pellet was dried out and
113 resuspended in TE buffer (Tris-HCl 10mM pH7.5, EDTA 0.1mM). The DNA was amplified using the Tpersonal
114 Thermocycler (Biometra, Analytik Jena AG, Jena, Germany). Two sets of primers were used to amplify the

115 targets sequences: HCAR1 forward TTCTGCTTTCACATGAAGACC, HCAR1 reverse CAGAACAAGATGATTGTCAGG,
116 and Neomycin forward GCAGCGCATCGCCTTCTATC, Neomycin reverse GATATCAGGTGGACAAGTCC.

117 Quantitative RT-PCR

118 Brains from WT (n=3) and HCAR1 KO (n=3) mice (1-month old) were dissected in 1mM MgCl₂ RNase-free PBS,
119 then frozen in liquid nitrogen, and kept at -80°C until use. RNA extraction from tissue or cultured neurons was
120 performed using the commercial Rneasy Mini Kit (Qiagen, Basel, Switzerland) and 1µg/µl was used for reverse
121 transcription to cDNA with the High capacity cDNA Reverse Transcription Kit (Applied Biosystems, California,
122 USA). The cDNA was amplified by quantitative RT-PCR (qRT-PCR) using the Power SYBR Green PCR Master mix
123 (BioRad, California, USA), with specific primers for the target genes at 200nM (HCAR1:
124 GGGGACTGTGTATCTTCTGA, GAGTCTTGGTGTAGAATTTGG; GAPDH: TCCATGACAACCTTGGCATTG,
125 CAGTCTTCTGGGTGGCAGTGA). Samples were run in triplicates and negative controls were run for each target
126 gene. All reactions were performed on a CFX96 Touch Real-time PCR detection system (BioRad). Relative
127 mRNA expression was quantified by using the comparative CT method, and results are shown as the fold
128 change using the 2CT formula (Livak and Schmittgen, 2001).

129 Immunohistochemistry

130 Primary cortical neurons from mRFP-HCAR1 mice (n=2) grown on coverslips were fixed with 4%
131 paraformaldehyde in phosphate-buffered solution (PBS) for 15 minutes on ice. Cells were pre-incubated with
132 15% serum and 0.05% Triton X-100 and subsequently incubated overnight with the primary mouse anti-NeuN
133 antibody (Catalog # MAB377, 1:200, Merck-Millipore, Darmstadt, Germany) and rabbit anti-mRFP (Catalog #
134 600-401-379, 1:100, Rockland Immunochemicals, Pottstown, PA, USA). Cells were incubated with the
135 appropriate secondary antibodies, *i.e.* Alexa Fluor 488-conjugated donkey anti-mouse IgG (Catalog #
136 ab105105, 1:200, Abcam, Cambridge, UK) and Alexa Fluor 594-conjugated donkey anti-rabbit IgG (Catalog #
137 ab150076, 1:200, Abcam). Brain sections from 1 month-old WT (n=6) and HCAR1 KO (n=5) mice were obtain
138 from mice anesthetized with sodium-pentobarbital (150mg/kg/intraperitoneally) and transcardially perfused

139 with 4% paraformaldehyde. The brains were sliced in a sagittal or coronal plane using a vibratome (Leica,
140 VT1000S), or cryoprotected in 30% sucrose and sliced using a microtome (Microm, HM 400), in both cases
141 30µm-thick slices were obtained. Slices were pre-incubated with 15% donkey serum and 0.3% Triton X-100
142 and subsequently incubated with the primary antibody overnight (see **Table 1-1**). In sequence, slices were
143 incubated with the appropriate secondary antibody (see **Table 1-2**).

144 Nuclei were stained using Hoechst (Invitrogen). Negative controls were performed in the absence of
145 primary antibodies. Coverslips and slices were mounted in Fluorsave mounting medium (Merck-Millipore).
146 Coverslips were analyzed using the Leica TCS SP5 confocal microscope (Leica, Wetzlar, Germany). Brain
147 sections were analyzed using the Zeiss LSM 710 confocal microscope (Zeiss, Oberkochen, Germany).

148 Western blot

149 Western blot was performed as previously described (Grishchuk et al., 2011), using WT (n=4) and HCAR1 KO
150 (n=4) cortex, hippocampus and cerebellum. Briefly, the different brain regions were dissected and then stored
151 at -20°C in lysis buffer, containing (mM): HEPES 20, pH 7.4, NaCl 10, MgCl₂ 3, EGTA 2.5, dithiothreitol 0.1, NaF
152 50, Na₃VO₄ 1, 1% Triton X-100 and a protease inhibitor cocktail (Roche, 1187350001). Protein concentration
153 was determined using a Bradford assay. Proteins (30–40 µg) were separated on 12% polyacrylamide gels and
154 analyzed by immunoblotting. Primary antibodies (see **Table 1-1**) were diluted in blocking buffer with 0.001%
155 PBS Tween-20 and incubated overnight at 4°C. Secondary antibodies (see **Table 1-2**) were diluted in blocking
156 buffer and incubated for 1h. Protein bands were visualized with the Odyssey Infrared Imaging System (LICOR,
157 NE, USA) or by using the enhanced chemiluminescence (ECL) method, using 200µl of ECL substrate
158 (SuperSignal West Dura Extended Duration Substrate, ThermoFisher Scientific). Odyssey v1.2 software (LICOR)
159 or Fujifilm Luminescent Image Analyzer (LAS 4000 mini) were used for analysis. Values were normalized with
160 respect to actin.

161 Live cell microscopy

162 Intracellular calcium imaging was carried out on an upright epifluorescence microscope (FN1, Nikon, Tokyo,
163 Japan) using a 40X 0.8 N.A water-immersion objective lens. Fluorescence excitation wavelengths were selected
164 using a fast filter wheel (Sutter Instr., Novato, CA) and fluorescence was detected using an Evolve EMCCD
165 camera (Photometrics, Tucson, AZ). Digital image acquisition and time series were computer-controlled using
166 the Metafluor software (RRID:SCR_014294). Up to 8 individual neurons were simultaneously analyzed in the
167 field of view. Intracellular calcium was measured using Fluo-8 AM (5 μ M, Abcam) loaded for 15 min at 37°C, in
168 a HEPES-buffered balanced solution containing (mM): NaCl 160, KCl 5.4, HEPES 20, CaCl₂ 1.3, MgSO₄ 0.8,
169 NaH₂PO₄ 0.78, glucose 20, pH 7.4 (adjusted with NaOH), supplemented with 0.1% Pluronic F127 (Molecular
170 Probes, Eugene, OR). Fluorescence was excited at 490nm and detected at >515nm, with an acquisition rate of
171 6-7Hz. Fluorescence intensity was measured over time in regions of interest delineating neuronal soma using
172 Metafluor. Calcium transients were analyzed using Mini Analysis 6.0.3 (RRID:SC_002184), which includes an
173 algorithm for the detection of complex and multiple events giving the possibility to detect overlapping or
174 closely occurring peaks, thus allowing the analysis of the frequency of spontaneous calcium spikes under
175 different experimental conditions.

176 FRET measurements of intracellular cAMP levels were carried out measured in cells expressing Epac2-
177 camps, 48 hours after transfection on an epifluorescence inverted microscope (Zeiss) equipped with an image
178 splitter (DV2, Photometrics, Tucson, AZ, USA), using a high numerical aperture fluorescence objective (40X 1.3
179 N.A. oil-immersion). Fluorescence excitation wavelengths were selected via fast holographic monochromator
180 (Polychrome II, Till Photonics, Planegg, Germany) coupled to a Xenon lamp and fluorescence was detected
181 using an EM CCD camera (LUCA-R, Andor, Belfast, UK). Digital image acquisition was performed using the
182 software Metafluor. One individual neuron was imaged in the selected field of view. Fluorescence was excited
183 at 430nm and detected at 475nm and at 530nm, for CFP and YFP respectively, with an acquisition rate of
184 0.2Hz. The region of interest from single cells YFP and CFP fluorescence intensities were extracted from the

185 CFP/YFP ratio using the Metafluor software. A decrease in FRET ratio signal reflects a decrease in the
186 intracellular cAMP levels.

187 Electrophysiological recordings

188 Patch-clamp recordings were made using borosilicate glass pipettes (5–6 M Ω), filled with intracellular solution
189 containing (in mM): K-gluconate 135, NaCl 5, Na-phosphocreatine 5, MgCl₂ 1, EGTA 1, HEPES 10, Mg-ATP 2,
190 and Na₃-GTP 0.4, pH 7.2 (adjusted with KOH). Recordings were made with a Multiclamp 700B amplifier
191 (Molecular Devices). Data were acquired with a Digidata 1440A (Molecular Devices), at 10kHz sampling rate,
192 controlled with pCLAMP 10 software (RRID:SCR_011323) and analyzed with Clampfit (RRID:SCR_011323) and
193 Mini Analysis (RRID:SCR_002184). The criterion for experiment inclusion in was based on the verification of
194 stable access resistance and leak current (<200pA at –70 mV in control solution).

195 Miniature excitatory post-synaptic currents (mEPSCs) were recorded at –70 mV in voltage-clamp in gap-
196 free mode. A stabilization period of 5 min was routinely allowed after establishment of the whole-cell
197 configuration. Experiments were performed in presence of 1 μ M tetrodotoxin (TTX) and 60 μ M bicuculline.
198 mEPSCs were recorded for 10 minutes in the absence and in the presence of HCAR1 agonist and the last 5
199 minutes were analyzed. Cells included in the analysis had a membrane potential \leq –55 mV, stable access
200 resistance, and recovery after washout.

201 We further assessed cell passive properties and firing frequency of WT neurons in control conditions and
202 after HCAR1 activation. The resting membrane potential (RMP) was measured in current clamp mode after the
203 whole cell configuration was established. The input resistance (R_N) was determined from the linear slope of
204 the current-voltage relationship around the RMP, obtained by a series of 160-ms current steps (starting at -
205 140pA with 30pA increments). The rheobase was determined as the minimal current amplitude able to evoke
206 an action potential (AP), and was obtained by applying 3-sec steps of positive current (starting at 0pA, 50pA
207 increments). The firing frequency was assessed as the number of AP evoked in response to 1-sec current
208 injection steps (0pA-450pA, 50pA increments). AP frequency was measured as the number of AP in response

209 to 150pA current injection. The membrane time constant was estimated by fitting an exponential function to a
210 voltage step of -5mV.

211 Paired pulse ratio (PPR) experiments were measured using a pipette solutions containing (in mM): CsF
212 121.6, CsCl 8.4, Na-phosphocreatine 5, EGTA 1, HEPES 10, Mg-ATP 2, Na₃-GTP 0.4, and QX-314Cl 1, pH 7.2
213 (adjusted with CsOH). Neurons were voltage-clamped at -70mV in the whole-cell configuration. Stimulation
214 was performed using a Pt-Ir concentric bipolar electrodes (Microprobes, MD, USA. Model CEA3, tip diameter
215 2-3µm) placed near the recorded neuron and connected to an Iso-Flex stimulus isolator (A.M.P.I, Jerusalem,
216 Israel). The minimum stimulation intensity able to trigger a single evoked EPSC was determined in the range
217 0.4-1mA. Two consecutive 1ms stimuli were applied with an interval of 50ms.

218 Solutions and drugs

219 CO₂/bicarbonate-buffered experimental solutions contained (mM): NaCl 135, KCl 5.4, NaHCO₃ 25, CaCl₂ 1.3,
220 MgSO₄ 0.8, NaH₂PO₄ 0.78, glucose 5, bubbled with 5% CO₂/95% air. Glucose was maintained in a non-limiting
221 fashion (5mM) in all solutions. Control extracellular solutions and solutions containing tested drugs were
222 gravity fed at 1ml/min and at 35°C. The pH of CO₂-equilibrated solutions was 7.4 and was not altered by the
223 added L-lactate (Bozzo et al., 2013). L-lactate, 3,5-DHBA, 3Cl-HBA, 9-(tetrahydro-2-furany)-9H-purin-6-amine
224 (SQ 22536), baclofen, guanfacine, gallein, and QX-314Cl were obtained from Sigma (Buchs, Switzerland). H-89
225 dihydrochloride (H-89), N₆-cyclopentyladenosine (CPA), (1-[6-[[[(17β)-3-methoxyestra-1,3,5(10)-trien-17-
226 yl]amino]hexyl]-1H-pyrrole-2,5-dione) (U73122) and bicuculline were obtained from Tocris (Bio-Techne, Zug,
227 Switzerland). Forskolin was obtained from Biomol (Anawa Trading, Zurich, Switzerland) and TTX was obtained
228 from BioTrend (Anawa Trading, Wangen, Switzerland). All drugs were diluted in CO₂/bicarbonate-buffered
229 solution to their final concentration and perfused in the same conditions as the control.

230 Experimental design and statistical significance

231 Immunohistochemistry data quantification was performed using the ImageJ software (RRID:SCR_003070). We
232 first identified Hoechst-stained nuclei in the field, allowing us to assess the number of cells. We then

233 determined cells that were NeuN and/or mRFP-positive to assess the number of neurons that were expressing
234 mRFP. For each independent experiment, three different fields of view were analyzed. Result of the
235 quantification is shown as percentage of Hoechst positive cells.

236 In order to assess HCAR1 functional role in neuronal activity, experiments were performed using a
237 sequential application of drugs. Each individual experiment represents responses obtained by the application
238 of the tested drugs, one following the other, on the same cells followed by washout with the control solution.
239 Statistical analyses were performed using the KaleidaGraph software (RRID:SCR_014980). Data are means \pm
240 SEM and are represented as percentage compared to control, n represents the number of independent
241 experiments. Data normality was checked using the Shapiro-Wilk test.

242 When more than one condition was tested on the same experiment comparisons were made using one-
243 way ANOVA followed by Bonferroni correction for each experimental group to assess statistical significance
244 against respective control, and among the tested conditions. When only one condition was tested the paired
245 or non-paired t-test was performed to assess statistical significance. *, **, and *** refer to *P* values lower than
246 0.05, 0.01 and 0.001, respectively. Only experiments where the effect of the tested drugs could be washed out
247 were taken into consideration for analysis.

248 **Results**249 *HCAR1 expression in neurons*

250 Localization of HCAR1 protein in neurons has been reported by us and other research groups based on
251 immunohistochemistry (Bozzo et al., 2013; Lauritzen et al., 2014). In this study, qRT-PCR was used to assess
252 HCAR1 mRNA expression in primary neuronal cultures at DIV 14 (**Fig. 1a**) from WT mice. **Fig. 1b** shows
253 genotyping results of WT and HCAR1 KO mice. In the gene construct of HCAR1 KO mice the coding sequence of
254 HCAR 1 was replaced by a cassette containing the lacZ and the neomycin resistance genes (Ahmed et al.,
255 2010). Samples from WT show a PCR HCAR1 band corresponding to 470bp product, whereas the ones from
256 HCAR1 KO animals have a neomycin only 800bp product band. In a next phase, we wanted to investigate the
257 HCAR1 protein expression and localization in primary cultured neurons. For this purpose we took advantage of
258 the HCAR1 KO mice, not available in our first studies, to assess the specificity of commercial antibodies. **Table**
259 **1** shows that out of 9 commercial antibodies raised against different epitopes, tested by Western blot and/or
260 immunohistochemistry, none displayed convincing absence of signal in HCAR1 KO tissue. To circumvent this
261 issue, we used a transgenic mouse that expresses monomeric red fluorescent protein (mRFP) under
262 the HCAR1 promoter (Ahmed et al., 2010). This fluorescent reporter protein is not targeted to the plasma
263 membrane but spreads in the cytoplasm, allowing us to identify the cells which endogenously express the
264 HCAR1 transcripts. In primary neurons from mRFP-HCAR1 mice, all Hoechst positive cells were also mRFP-
265 HCAR1 positive. Among these cells around 80% were also positive for NeuN (**Fig. 1c,d**). This result indicates
266 that these cultured neurons express mRFP-HCAR1. The 20% of the cells that were mRFP-HCAR1 positive but
267 NeuN negative, could represent cells that are not mature neurons and that also express HCAR1.

268 *HCAR1 KO animals show normal general behavior*

269 According to previous studies, HCAR1 KO mice do not show obvious abnormalities when compared to WT,
270 which includes no difference in body weight (Ahmed et al., 2010) or locomotion when exposed to high-

271 intensity interval exercises (Morland et al., 2017). We extended the phenotype analysis and performed a basic
272 behavioral neurological screening in these animals. We did not find differences in the quantitative
273 observations obtained with the Phenotyper cage nor during the free observation (**Table 2**). Neither WT nor
274 HCAR1 KO animals presented traces of compulsive licking, self-destructive biting, repulsion or convulsions.
275 No differences were observed in the grip strength test ($t(22) = 0.49$, $p=0.63$, unpaired t-test) and in the
276 hindpaw clasping test (none of the mice failed the test; WT, $n=12$ animals; HCAR1 KO, $n=12$ animals).

277 Activation of HCAR1 decreases mEPSC frequency and excitability

278 In a next phase, we evaluated the effects of HCAR1 activation on basal neurotransmission using the whole-cell
279 patch-clamp technique. **Fig. 2a** shows representative electrophysiological traces of mEPSCs recorded from
280 neurons of WT and HCAR1 KO mice. We observed a significant decrease (~50%) in mEPSCs frequency in the
281 WT group during HCAR1 activation by its agonist 3Cl-HBA ($40\mu\text{M}$; $F(2,6)=12.92$, $p=0.0013$, ANOVA). 3Cl-HBA
282 application did not alter the mean amplitude ($F(2,6)=5.84$, $p=0.562$, ANOVA) or kinetics (Rise: $t(6)= -1.41$, $p=$
283 0.22 ; Decay $t(6)= 0.19$, $p= 0.85$; Area: $t(6)= -0.77$, $p=0.48$, paired t-test) of mEPSCs (**Fig. 2b,c**). Importantly, the
284 frequency ($F(2,5)=0.09$, $p=1$, ANOVA), amplitude ($F(2,5)=0.23$, $p=1$, ANOVA) and kinetics (Rise: $t(5)= 1.39$, $p=$
285 0.22 ; Decay $t(5)= 0.87$, $p= 0.42$; Area: $t(5)= -0.63$, $p=0.56$, paired t-test) of mEPSCs were not influenced by
286 HCAR1 activation in neurons from HCAR1 KO mice (**Fig. 2c**). These results are a first indication of a presynaptic
287 mechanism induced by HCAR1. To further test this hypothesis, we performed a PPR experiment before and
288 after HCAR1 activation. These experiments revealed a significant increase in the PPR value ($t(6) = -5.18$,
289 $p=0.002$, paired t-test) (**Fig. 2d**), supporting the notion that HCAR1 has a presynaptic component.

290 However, previous works indicated that HCAR1 activation modulates passive properties and decreases
291 the firing frequency of rat CA1 pyramidal neurons (Herrera-Lopez and Galvan, 2018). Thus, we investigated
292 whether HCAR1 activation could modulate intrinsic properties of mouse cortical neurons as well. We observed
293 that activation of HCAR1 with 3Cl-HBA ($40\mu\text{M}$) decreased firing frequency by 45 % ($t(4)= 6.53$, $p= 0.003$, paired
294 t-test) (**Fig. 2e**), as previously observed by Herrera-Lopez and Galvan (2018). **Table 3** further shows that

295 activation of HCAR1 causes a significant decrease in input resistance ($t(4) = 4.35$, $p = 0.01$, paired t-test) and
296 membrane time constant ($t(4) = -3.69$, $p = 0.02$, paired t-test), increases the rheobase current ($t(4) = -4.09$, $p =$
297 0.01 , paired t-test), and hyperpolarizes the RMP ($t(4) = 3.41$, $p = 0.03$, paired t-test). These experiments
298 indicate that HCAR1 activation induces changes in the intrinsic membrane properties of mouse cortical
299 neurons, eliciting a decrease in excitability in addition to a presynaptic mechanism.

300 Activation of HCAR1 decreases neuronal calcium spiking frequency

301 The spontaneous spiking activity of primary cortical neurons was then measured by calcium imaging. As
302 previously demonstrated (Bozzo et al., 2013), intracellular calcium transients directly correlate with action
303 potentials in single neurons. This approach offers the advantage of recording a number of cells in parallel
304 without altering the intracellular solute composition compared with the whole-cell patch-clamp method.

305 Activation of HCAR1 was tested in neurons obtained from both WT and HCAR1 KO mice. HCAR1 is
306 endogenously activated by L-Lactate in neurons with an apparent IC_{50} of 4.2mM (Bozzo et al., 2013). For these
307 experiments, we tested the endogenous ligand L-lactate, as well as two specific, non-metabolized agonists of
308 HCAR1, namely 3,5-DHBA and the newer, higher affinity agonist 3Cl-HBA. **Fig. 3a** shows that application of L-
309 lactate (5mM) on neurons from WT mice led to a decrease in spontaneous spiking frequency by approximately
310 40%, as observed before (Bozzo et al., 2013). We then tested the higher affinity agonist 3Cl-HBA and
311 performed a log-dose analysis of its effect on neuronal activity (**Fig. 3b**). 3Cl-HBA caused a decrease in spiking
312 frequency with an IC_{50} of $21.6 \pm 6.1\mu M$ ($n = 23$ exp.), virtually identical to the $22\mu M$ potency originally found
313 with the mouse HCAR1 isoform (Dvorak et al., 2012). **Fig. 3c** summarizes this series of experiments and shows
314 that L-lactate ($F(2,15) = 555.95$, $p < 0.0001$, ANOVA), 3,5-DHBA ($F(2,15) = 429.20$, $p < 0.0001$, ANOVA), and 3Cl-HBA
315 ($F(2,2) = 224.57$, $p < 0.0001$, ANOVA) strongly decreased spiking frequency. In sharp contrast, neither L-lactate
316 ($F(2,15) = 45.71$, $p = 0.26$, ANOVA), 3,5-DHBA ($F(2,11) = 47.59$, $p = 0.22$, ANOVA), nor 3Cl-HBA ($F(2,4) = 3.93$, $p = 1$,
317 ANOVA) altered spontaneous spiking frequency in neurons prepared from HCAR1 KO mice. This result is a
318 strong indication that HCAR1 activation is responsible and required for the modulatory effects of L-lactate on

319 neuronal network spontaneous activity. It should be added that in control conditions, neurons obtained from
320 HCAR1 KO displayed an approximately two-fold higher basal activity compared to WT neurons ($t(30) = -4.83$,
321 $p < 0.0001$, unpaired t-test) (**Fig. 3d**), suggesting that HCAR1 might have a role in the tonic inhibition of neuronal
322 activity.

323 Intracellular HCAR1 signaling pathways in neurons

324 HCA receptors have been reported to be coupled to G_i proteins in the adipose tissue (Liu et al., 2009). Our
325 group previously demonstrated that the lactate effect on cortical neurons is sensitive to pertussis toxin, which
326 supports the notion that HCAR1 in neurons decreases neuronal activity through the G_i protein pathway (Bozzo
327 et al., 2013). Therefore, we investigated if the downstream effectors of G_i protein were involved in the
328 decrease of neuronal activity induced by HCAR1 activation.

329 Using calcium imaging, we analyzed the effect of HCAR1 activation on neuronal spiking frequency upon
330 pharmacological manipulation of the intracellular pathways known to follow the activation of G_i proteins.
331 Activation of AC by forskolin (10 μ M) caused a ~30% increase in spiking activity in WT neurons, which was
332 reversed by concomitant activation of HCAR1 ($F(3,4) = 23.16$, $p < 0.0001$, ANOVA) (**Fig. 4a**). In comparison,
333 forskolin was found to have a stronger stimulatory effect on neurons from HCAR1 KO animals, suggesting a
334 tonic inhibitory effect operated by HCAR1 on AC. Moreover, the HCAR1 agonist 3,5-DHBA had no effect on
335 forskolin-induced activity of these neurons ($F(3,2) = 24.89$, $p = 1$, ANOVA) (**Fig. 4a**). Conversely, inhibition of AC
336 with SQ22536 (10 μ M) decreased neuronal spiking activity by ~40%. In this situation, under AC inhibition,
337 HCAR1 activation did not cause further spiking activity decrease ($F(3,6) = 15.39$, $p = 1$, ANOVA) (**Fig. 4b**). These
338 results indicate that HCAR1 activation impact AC in neurons. Live-cell imaging of cAMP levels in neurons was
339 then performed using the FRET sensor Epac2-camps. **Fig. 4c** shows that forskolin application caused a rapid
340 increase in FRET response, corresponding to cAMP level rise. This cAMP level increase was efficiently reversed
341 by the application of the HCAR1 agonist 3CI-HBA ($t(5) = 6.62$, $p = 0.001$, paired t-test) (**Fig. 4c&d**). We then
342 tested PKA as one of the main downstream targets of AC-cAMP. To this aim, we used H-89 (1 μ M) to inhibit

343 PKA, which led to a decrease in neuronal network activity. Under PKA blockade, activation of HCAR1 using 3,5-
344 DHBA did not cause a further decrease in spiking activity ($F(3,6)=80.75$, $p=0.61$, ANOVA) (**Fig. 4e**). Taken
345 together, these experiments demonstrate that HCAR1 action on neuronal spiking activity involves the
346 inhibition of AC, causing a decrease in cAMP levels and in turn of PKA activity.

347 *HCAR1 interacts with G_i coupled receptors to modulate neuronal activity*

348 A characteristic feature of GPCRs is their ability to cross-talk with other GPCRs at the level of their intracellular
349 pathways (Werry et al., 2003). These interactions significantly complexify their effects on cellular or network
350 targets. We therefore asked whether HCAR1 is capable of functionally interacting with other G_i-coupled
351 receptors, such as the adenosine A1 receptor (A1R), the GABA_B receptor (GABA_BR) and the α_{2A} adrenoreceptor
352 (α_{2A} R). To address this question, we used calcium imaging to monitor neuronal activity upon the sequential
353 activation of HCAR1 and one of the G_i coupled receptors. We found that activation of HCAR1 with 3,5-DHBA
354 decreased neuronal spiking frequency, as shown above, and the subsequent co-activation of HCAR1 and A1R
355 using CPA induced a further decrease in neuronal spiking frequency ($F(3,3)=20.57$, $p=0.046$, ANOVA) (**Fig. 5a**).
356 After washout of the drugs, spiking activity returned to its original frequency (*not shown*). The same apparent
357 additive inhibition of spiking was observed when investigating the cooperation of HCAR1 with GABA_BR or with
358 α_{2A} R, which were activated using baclofen and guanfacine, respectively (**Table 4**). It is expected that if
359 activation of HCAR1 and the other G_i-coupled receptors are independent, reversing the order of agonist
360 application should result in the same combined inhibition of neuronal spiking. We tested this hypothesis by
361 first stimulating A1R and immediately after co-activating HCAR1. Unexpectedly, when A1R was first activated,
362 the subsequent co-activation of HCAR1 partially reversed the inhibition induced by A1R alone ($F(3,3)=32.09$,
363 $p=0.007$, ANOVA) (**Fig. 5b**). We repeated the same protocol with GABA_BR or α_{2A} R and the same pattern was
364 observed (**Table 4**). To ascertain that this effect was specifically brought about by HCAR1, we repeated these
365 experiments with neurons prepared from HCAR1-KO animals. **Fig. 5c** ($F(3,3)=193.06$, $p=1$, ANOVA) and **Table 4**
366 show that in neurons lacking HCAR1 situation no such interaction was observed, indicating that the observed

367 effects were indeed mediated by the HCAR1. We then asked whether this reversal effect caused by HCAR1
368 activation was generic to all G_i -coupled receptors. We repeated the experiments depicted above for
369 A1R/GABA_BR, A1R/ α_2 AR, and α_2 AR/GABA_BR pairs. Results listed in **Table 5** indicate that this reversal of
370 inhibition was not observed among these receptor pairs, which did not recapitulate the observations made
371 with HCAR1. This indicates that this reversal of frequency decrease is a distinct property of HCAR1 activation.

372 Overall, these experiments revealed that depending on which receptor is activated first in sequence,
373 different levels of inhibition of spiking frequency are obtained upon HCAR1 co-activation with other G_i coupled
374 receptors, highlighting the complexity of the modulation of neuronal activity operated by HCAR1.

375 *The $G_{i\beta\gamma}$ -PLC pathway is involved in the interaction of HCAR1 with G_i coupled receptors*

376 Although the G_i pathway is classically known for its ability to inhibit AC, both $G_{i\alpha}$ and $G_{i\beta\gamma}$ subunits can
377 transduce signals. One of the key effectors directly regulated by $G_{\beta\gamma}$ subunits is phospholipase C (PLC). PLC
378 catalyzes the hydrolysis of phosphatidylinositol 4,5-biphosphate (PIP₂) to generate 1,2-diacylglycerol and
379 inositol 1,4,5-trisphosphate (IP₃), which binds to its receptor on the endoplasmic reticulum (Rhee, 2001). Thus,
380 we investigated if PLC activation induced by the $G_{i\beta\gamma}$ subunit was involved in the observed effect on the
381 functional interaction between HCAR1 and G_i coupled receptors. In experiments repeating the sequence of
382 agonist application presented in **Fig. 5b**, inhibition of $G_{i\beta\gamma}$ subunit using gallein suppressed the partial reversal
383 of inhibition induced by the co-activation of A1R and HCAR1 ($F(3,3)=84.71$, $p=1$, ANOVA) (**Fig. 5d**). The same
384 approach was applied to test the involvement of $G_{i\beta\gamma}$ subunit on the cooperation observed between GABA_BR or
385 α_2 AR and HCAR1. As indicated in **Table 6**, in both cases, gallein prevented the HCAR1 agonist from reversing
386 the inhibition induced by GABA_BR or α_2 AR stimulation. In all experiments, after washout of gallein and
387 agonists, the spiking frequency returned to its control value (*not shown*). These results support the
388 involvement of $G_{\beta\gamma}$ subunit in the observed effects.

389 PLC is classically activated by the $G_{q\alpha}$ and $G_{q\beta\gamma}$ proteins dissociated from G_q -coupled receptors. However,
390 PLC was also shown to be activated by $G_{i\beta\gamma}$ proteins released from G_i proteins (Tomura et al., 1997; Mizuta et

391 al., 2011). Thus, we investigated if PLC was the downstream mechanism activated by the $G_{i\beta\gamma}$ subunit and
392 involved in the interplay between HCAR1 and other G_i -coupled receptors. Application of U73122, the inhibitor
393 of PLC, prevented HCAR1 agonist from reversing the spiking frequency decrease caused by A1R
394 ($F(3,3)=1621.87$, $p=1$, ANOVA)(**Fig. 5e**), $GABA_B$ R, or α_2 AR (**Table 6**). After washout of U73122 and agonists, the
395 spiking frequency returned to its control value (*not shown*). These results indicate that the partial reversal of
396 inhibition caused by HCAR1 activation under these conditions involves $G_{i\beta\gamma}$ and PLC. As a control, we assessed
397 the effect of $G_{i\beta\gamma}$ and PLC blockade on the HCAR1 signaling itself. Blockade of $G_{i\beta\gamma}$ was sufficient to decrease the
398 inhibitory action of HCAR1 ($F(3,3)=84.10$, $p= 0.008$, ANOVA) (**Fig. 5f**). In contrast, inhibition of PLC did not
399 influence the effect of HCAR1 activation alone ($F(3,3)=59.38$, $p= 1$, ANOVA) (**Fig. 5g**). Thus, it appears that the
400 $G_{i\beta\gamma}$ subunit is necessary for the modulatory effects of HCAR1, but that PLC is only required upon activation of
401 an additional G_i -coupled receptor. Taken together, these results indicate that HCAR1 interacts with G_i -coupled
402 receptors in a complex but specific manner, through both its $G_{i\alpha}$ and $G_{i\beta\gamma}$ subunits.

403 **Discussion**

404 In this study, we demonstrate that HCAR1 in neurons is necessary for the modulation of spontaneous neuronal
405 activity induced by L-lactate. We observed that HCAR1 activation with L-lactate induced a reversible decrease
406 in the neuronal calcium spiking activity by approximately 40%, in line with first indications reported by our
407 group (Bozzo et al., 2013). Activation of HCAR1 with non-metabolized agonists, 3,5-DHBA and 3CI-HBA, also
408 decreased neuronal calcium spiking , as well as the mEPSCs frequency and AP firing frequency by similar
409 amounts. We observed that HCAR1 activation induced changes in PPR and modulated neuronal intrinsic
410 properties. As decisive arguments for the critical role of HCAR1, the activity of HCAR1 KO neurons was totally
411 insensitive to HCAR1 agonists and the basal activity of these neurons was higher than that of neurons from WT
412 mice. HCAR1 is therefore required for the non-metabolic effects of L-lactate on spontaneous and tonic
413 neuronal activity.

414 HCAR1 pattern of expression in the CNS was first described to localize at the membrane of excitatory
415 synapses of the hippocampus and cerebellar cortex (Lauritzen et al., 2014). However, because of the
416 questionable specificity of HCAR1 antibodies currently available (Table 1 and Michel et al., 2009; Wallenius et
417 al., 2017), the precise HCAR1 cellular and regional localization in the brain remains uncertain. At this stage, one
418 can find evidence for HCAR1 brain expression from in situ hybridization (the Allen Brain Atlas,
419 <http://www.brain-map.org>), proteomics (Uniprot database, <https://www.uniprot.org>) and transcriptomics
420 (Zhang et al., 2014). HCAR1 expression in the brain was estimated to be one order of magnitude lower than in
421 adipose tissue, where it was initially identified (Lauritzen et al., 2014).

422 In the CNS, several studies provided evidence for a signaling role of L-lactate. Suzuki et al. (2011) reported
423 that long-term memory formation and maintenance are mechanisms for which L-lactate plays an essential
424 role. Yang et al. (2014) showed that L-lactate stimulates the expression of synaptic plasticity-related genes. *In*
425 *vivo* administration of L-lactate inhibited firing in the hippocampus (Gilbert et al., 2006), and in the subfornical
426 organ 5mM L-lactate decreased spiking activity of GABAergic neurons (Shimizu et al., 2007) . A recent study

427 showed that 5mM L-lactate and the HCAR1 agonist 3,5-DHBA, decreased neuronal activity in a non-metabolic
428 way by modulating neuronal intrinsic excitability, significantly blocking fast inactivating sodium current, and
429 increasing the delay from inactivation to a conducting state of the sodium channel in rat CA1 pyramidal
430 neurons (Herrera-Lopez and Galvan, 2018). L-lactate also plays an important protective role in cerebral
431 ischemia. It was observed that intracerebral L-lactate administration, decreases the lesion size and improves
432 the neurological outcome (Berthet et al., 2009). A follow-up study showed that both L-lactate and D-lactate,
433 which is poorly metabolized but also activates HCAR1, equally provides neuroprotection in ischemic
434 conditions, and that 3,5-DHBA reduces cell death, suggesting that L-lactate protective functions involves
435 HCAR1 activation (Castillo et al., 2015). HCAR1 was also shown to be involved in enhanced brain angiogenesis
436 linked with physical activity (Morland et al., 2017).

437 By using electrophysiological recordings, we observed that HCAR1 activation decreased the frequency of
438 mEPSCs, providing an indication for a presynaptic action of this receptor. This conclusion was supported by
439 PPR experiments. To our knowledge, it is the first evidence of a presynaptic effect of HCAR1. A change in
440 excitability has also been observed by others in rat hippocampal neurons (Herrera-Lopez and Galvan, 2018).
441 We investigated if this was the case in mouse cortical neurons. Activation of HCAR1 reduced input resistance
442 and firing frequency, increased the rheobase current, and caused RMP hyperpolarization. These changes in
443 excitability possibly involve the modulation of potassium conductances and of fast inactivating sodium
444 currents reported by Herrera-Lopez and Galvan (2018). These experiments provided evidence supporting a
445 presynaptic as well as a postsynaptic effect of HCAR1.

446 In adipocytes, HCAR1 signals through a $G_{i\alpha}$ -protein pathway (Ge et al., 2008) and L-lactate mediates its
447 anti-lipolytic effect with an IC_{50} value of ~5mM (Cai et al., 2008; Liu et al., 2009). In the present study, we
448 investigated whether in cortical neurons $G_{i\alpha}$ -protein pathway and its canonical downstream effectors were
449 engaged for the observed inhibition of neuronal activity. Our group was able to reverse the inhibitory effect of
450 L-lactate on neuronal activity by applying pertussis toxin, an inhibitor of $G_{i\alpha}$ -proteins, which provided a first

451 indication for the involvement of G_i-coupled receptor mediated action of lactate in cortical neurons (Bozzo et
452 al., 2013). Here, we found evidence for the involvement of AC, as the enhancement of spiking activity by the
453 AC activator forskolin could be reversed by HCAR1 activation. Importantly, this did not happen in neurons from
454 HCAR1 KO mice. Conversely, inhibiting AC using SQ22536, decreased spontaneous spiking; however, HCAR1
455 activation had no further effect. By directly measuring cAMP in single living neurons using a cAMP FRET
456 biosensor, we found that the increase of cAMP level induced by AC activation was reversed by the HCAR1
457 agonist. This result is in agreement with the report made in rat hippocampal slices (Lauritzen et al., 2014). One
458 important downstream target of cAMP is PKA. We found that under PKA inhibition, HCAR1 activation did no
459 longer decrease neuronal spiking activity. Overall, these experiments indicate that the down-modulation of
460 spontaneous neuronal activity by HCAR1 activation requires a functional intracellular AC-cAMP-PKA signaling
461 pathway. Along these lines, cAMP is known to serve as a signal that modulates neuronal vesicular release
462 through PKA-dependent and PKA-independent mechanisms (Seino and Shibasaki, 2005). Moreover, it is known
463 that G_i-coupled receptors (*e.g.* A1R, GABA_BR, α₂AR) regulate neuronal excitability by inducing or modulating
464 ion currents such as various K⁺ conductances, including HCN (Wang et al., 2007), two-pore domain K⁺ channels
465 (Deng et al., 2009) , or GIRK channels (Breton and Stuart, 2017).

466 In several systems GPCRs have the properties to interact with each other, enabling them to operate a
467 much more complex modulation than individual transduction pathways acting independently (Werry et al.,
468 2003). It was shown that co-activation of two G_{i/o}-coupled receptors, *e.g.* A1 adenosine and cannabinoid CB1
469 receptors, reduces cAMP formation in rat hippocampus, which causes additive inhibitory effects on neuronal
470 activity (Serpa et al., 2009). Another example of intracellular interaction of combined G_i-coupled receptor
471 activation was found between adenosine A1 and group II metabotropic glutamate receptors: their sequential
472 activation did not lead to additive presynaptic inhibition, but to a mutual occlusion of effects on retinotectal
473 synapses (Zhang and Schmidt, 1999).

474 We therefore questioned whether HCAR1 follows such interaction patterns with other classical G_i-coupled
475 receptors. We selected the adenosine A1, GABA_B, and α_{2A}-adrenergic receptors, which are all G_i-coupled
476 receptors known to be expressed in cortical neurons and to signal through the decrease of AC activity, cAMP
477 levels, and PKA activity. When HCAR1 was stimulated first in sequence followed by the stimulation of the other
478 GPCR, an apparent additive decrease in spiking frequency was observed. However, when the order of receptor
479 activation was permuted, HCAR1 activation rather partly reversed the inhibitory effect of the first receptor.
480 The observation was made with all three receptors (adenosine A1, GABA_B, and α_{2A}-adrenergic receptors) and
481 was absent in HCAR1 KO neurons. This type of cooperation was not reproduced when selecting pairs among
482 these three GPCRs. Thus, HCAR1 appears to have distinctive actions on neuronal activity when activated in
483 combination with other receptors sharing similar transduction mechanisms.

484 The way HCAR1 is interacting with other GPCRs likely involves additional mechanisms than the canonical
485 AC-cAMP-PKA pathway. It was demonstrated that recombinant HCAR1 activation induces ERK1/2
486 phosphorylation through the activation of its G_{βγ}-subunit (Li et al., 2014). HCAR1 may therefore have the ability
487 to signal through both its G_{iα} and G_{iβγ} subunits. We postulated that the partial reversal of inhibition of G_i-
488 coupled receptors brought about by HCAR1 is mediated by G_{iβγ} subunits released from the G_i complex after
489 receptor stimulation. We found that blocking G_{iβγ} subunit not only reduced the inhibitory effect of HCAR1
490 alone, but also prevented the reversal of spiking inhibition observed when HCAR1 was activated in sequence
491 with another G_i-coupled receptor. In further support of this hypothesis, blockade of PLC, a downstream target
492 of G_{βγ} (Katz et al., 1992), also prevented the observed partial reversal of inhibition. However PLC seems to be
493 only engaged when HCAR1 is activated in sequence with another receptor, since PLC blockade did not alter the
494 effect of HCAR1 activation alone.

495 In this study, we demonstrate that lactate has the ability to modulate neuronal activity through HCAR1,
496 providing further support for the hypothesis that lactate, in addition to being an energy substrate for neurons,
497 can function as a gliotransmitter. HCAR1 mediates its effect through its G_{iα} subunit and its downstream

498 effectors, resulting in a decrease of neuronal excitability and consequent firing frequency (**Fig. 6**). The ability of
499 HCAR1 to functionally interact with other GPCRs through both $G_{i\alpha}$ and $G_{i\beta\gamma}$ subunits add a level of complexity to
500 its mechanism of action on neuronal activity, and implies that the outcome of its activation *in vivo* will depend
501 on whether other receptors of this class are active at any given time.

502 **References**

- 503 Abi-Saab WM, Maggs DG, Jones T, Jacob R, Srihari V, Thompson J, Kerr D, Leone P, Krystal JH, Spencer DD,
504 During MJ, Sherwin RS (2002) Striking differences in glucose and lactate levels between brain extracellular
505 fluid and plasma in conscious human subjects: effects of hyperglycemia and hypoglycemia. *J Cereb Blood*
506 *Flow Metab* 22:271-279.
- 507 Ahmed K, Tunaru S, Tang C, Muller M, Gille A, Sassmann A, Hanson J, Offermanns S (2010) An autocrine lactate
508 loop mediates insulin-dependent inhibition of lipolysis through GPR81. *Cell Metab* 11:311-319.
- 509 Barros LF (2013) Metabolic signaling by lactate in the brain. *Trends Neurosci* 36:396-404.
- 510 Berthet C, Lei H, Thevenet J, Gruetter R, Magistretti PJ, Hirt L (2009) Neuroprotective role of lactate after
511 cerebral ischemia. *J Cereb Blood Flow Metab* 29:1780-1789.
- 512 Blad CC, Tang C, Offermanns S (2012) G protein-coupled receptors for energy metabolites as new therapeutic
513 targets. *Nat Rev Drug Discov* 11:603-619.
- 514 Bozzo L, Puyal J, Chatton JY (2013) Lactate modulates the activity of primary cortical neurons through a
515 receptor-mediated pathway. *PLoS One* 8:e71721.
- 516 Breton JD, Stuart GJ (2017) GABAB receptors in neocortical and hippocampal pyramidal neurons are coupled
517 to different potassium channels. *Eur J Neurosci* 46:2859-2866.
- 518 Cai TQ, Ren N, Jin L, Cheng K, Kash S, Chen R, Wright SD, Taggart AK, Waters MG (2008) Role of GPR81 in
519 lactate-mediated reduction of adipose lipolysis. *Biochem Biophys Res Commun* 377:987-991.

- 520 Castillo X, Rosafio K, Wyss MT, Drandarov K, Buck A, Pellerin L, Weber B, Hirt L (2015) A probable dual mode of
521 action for both L- and D-lactate neuroprotection in cerebral ischemia. *J Cereb Blood Flow Metab* 35:1561-
522 1569.
- 523 Dalsgaard MK, Quistorff B, Danielsen ER, Selmer C, Vogelsang T, Secher NH (2004) A reduced cerebral
524 metabolic ratio in exercise reflects metabolism and not accumulation of lactate within the human brain. *J*
525 *Physiol* 554:571-578.
- 526 Deng PY, Xiao Z, Yang C, Rojanathammanee L, Grisanti L, Watt J, Geiger JD, Liu R, Porter JE, Lei S (2009)
527 GABA(B) receptor activation inhibits neuronal excitability and spatial learning in the entorhinal cortex by
528 activating TREK-2 K⁺ channels. *Neuron* 63:230-243.
- 529 Diaz-Garcia CM, Mongeon R, Lahmann C, Koveal D, Zucker H, Yellen G (2017) Neuronal Stimulation Triggers
530 Neuronal Glycolysis and Not Lactate Uptake. *Cell Metab* 26:361-374 e364.
- 531 Dienel GA, Ball KK, Cruz NF (2007) A glycogen phosphorylase inhibitor selectively enhances local rates of
532 glucose utilization in brain during sensory stimulation of conscious rats: implications for glycogen turnover.
533 *J Neurochem* 102:466-478.
- 534 Dvorak CA, Liu C, Shelton J, Kuei C, Sutton SW, Lovenberg TW, Carruthers NI (2012) Identification of
535 Hydroxybenzoic Acids as Selective Lactate Receptor (GPR81) Agonists with Antilipolytic Effects. *ACS*
536 *medicinal chemistry letters* 3:637-639.
- 537 Ge H, Weiszmann J, Reagan JD, Gupte J, Baribault H, Gyuris T, Chen JL, Tian H, Li Y (2008) Elucidation of
538 signaling and functional activities of an orphan GPCR, GPR81. *J Lipid Res* 49:797-803.
- 539 Gilbert E, Tang JM, Ludvig N, Bergold PJ (2006) Elevated lactate suppresses neuronal firing in vivo and inhibits
540 glucose metabolism in hippocampal slice cultures. *Brain Res* 1117:213-223.

- 541 Gladden LB (2004) Lactate metabolism: a new paradigm for the third millennium. *J Physiol* 558:5-30.
- 542 Grishchuk Y, Ginet V, Truttmann AC, Clarke PG, Puyal J (2011) Beclin 1-independent autophagy contributes to
543 apoptosis in cortical neurons. *Autophagy* 7:1115-1131.
- 544 Herrera-Lopez G, Galvan EJ (2018) Modulation of hippocampal excitability via the hydroxycarboxylic acid
545 receptor 1. *Hippocampus* doi: 10.1002/hipo.22958.
- 546 Husted AS, Trauelsen M, Rudenko O, Hjorth SA, Schwartz TW (2017) GPCR-Mediated Signaling of Metabolites.
547 *Cell Metab* 25:777-796.
- 548 Katz A, Wu D, Simon MI (1992) Subunits beta gamma of heterotrimeric G protein activate beta 2 isoform of
549 phospholipase C. *Nature* 360:686-689.
- 550 Lauritzen KH, Morland C, Puchades M, Holm-Hansen S, Hagelin EM, Lauritzen F, Attramadal H, Storm-Mathisen
551 J, Gjedde A, Bergersen LH (2014) Lactate receptor sites link neurotransmission, neurovascular coupling, and
552 brain energy metabolism. *Cereb Cortex* 24:2784-2795.
- 553 Li G, Wang HQ, Wang LH, Chen RP, Liu JP (2014) Distinct pathways of ERK1/2 activation by hydroxy-carboxylic
554 acid receptor-1. *PLoS One* 9:e93041.
- 555 Liu C, Wu J, Zhu J, Kuei C, Yu J, Shelton J, Sutton SW, Li X, Yun SJ, Mirzadegan T, Mazur C, Kamme F, Lovenberg
556 TW (2009) Lactate inhibits lipolysis in fat cells through activation of an orphan G-protein-coupled receptor,
557 GPR81. *J Biol Chem* 284:2811-2822.
- 558 Livak KJ, Schmittgen TD (2001) Analysis of relative gene expression data using real-time quantitative PCR and
559 the 2⁻(Delta Delta C(T)) Method. *Methods* 25:402-408.

- 560 Mächler P, Wyss MT, Elsayed M, Stobart J, Gutierrez R, von Faber-Castell A, Kaelin V, Zuend M, San Martin A,
561 Romero-Gomez I, Baeza-Lehnert F, Lengacher S, Schneider BL, Aebischer P, Magistretti PJ, Barros LF, Weber
562 B (2016) In vivo evidence for a lactate gradient from astrocytes to neurons. *Cell Metab* 23:94-102.
- 563 Michel MC, Wieland T, Tsujimoto G (2009) How reliable are G-protein-coupled receptor antibodies? *Naunyn*
564 *Schmiedebergs Arch Pharmacol* 379:385-388.
- 565 Mizuta K, Mizuta F, Xu D, Masaki E, Panettieri RA, Jr., Emala CW (2011) Gi-coupled gamma-aminobutyric acid-B
566 receptors cross-regulate phospholipase C and calcium in airway smooth muscle. *Am J Respir Cell Mol Biol*
567 45:1232-1238.
- 568 Morland C et al. (2017) Exercise induces cerebral VEGF and angiogenesis via the lactate receptor HCAR1. *Nat*
569 *Commun* 8:15557.
- 570 Nikolaev VO, Bunemann M, Hein L, Hannawacker A, Lohse MJ (2004) Novel single chain cAMP sensors for
571 receptor-induced signal propagation. *J Biol Chem* 279:37215-37218.
- 572 Offermanns S (2017) Hydroxy-Carboxylic Acid Receptor Actions in Metabolism. *Trends Endocrinol Metab*
573 28:227-236.
- 574 Pellerin L, Magistretti PJ (1994) Glutamate uptake into astrocytes stimulates aerobic glycolysis: a mechanism
575 coupling neuronal activity to glucose utilization. *Proc Natl Acad Sci USA* 91:10625-10629.
- 576 Rhee SG (2001) Regulation of phosphoinositide-specific phospholipase C. *Annu Rev Biochem* 70:281-312.
- 577 Seino S, Shibasaki T (2005) PKA-dependent and PKA-independent pathways for cAMP-regulated exocytosis.
578 *Physiol Rev* 85:1303-1342.

- 579 Serpa A, Ribeiro JA, Sebastiao AM (2009) Cannabinoid CB(1) and adenosine A(1) receptors independently
580 inhibit hippocampal synaptic transmission. *Eur J Pharmacol* 623:41-46.
- 581 Shimizu H, Watanabe E, Hiyama TY, Nagakura A, Fujikawa A, Okado H, Yanagawa Y, Obata K, Noda M (2007)
582 Glial Nax channels control lactate signaling to neurons for brain [Na⁺] sensing. *Neuron* 54:59-72.
- 583 Sotelo-Hitschfeld T et al. (2015) Channel-mediated lactate release by K(+)-stimulated astrocytes. *J Neurosci*
584 35:4168-4178.
- 585 Suzuki A, Stern SA, Bozdagi O, Huntley GW, Walker RH, Magistretti PJ, Alberini CM (2011) Astrocyte-neuron
586 lactate transport is required for long-term memory formation. *Cell* 144:810-823.
- 587 Tang F, Lane S, Korsak A, Paton JF, Gourine AV, Kasparov S, Teschemacher AG (2014) Lactate-mediated glia-
588 neuronal signalling in the mammalian brain. *Nat Commun* 5:3284.
- 589 Tomura H, Itoh H, Sho K, Sato K, Nagao M, Ui M, Kondo Y, Okajima F (1997) Betagamma subunits of pertussis
590 toxin-sensitive G proteins mediate A1 adenosine receptor agonist-induced activation of phospholipase C in
591 collaboration with thyrotropin. A novel stimulatory mechanism through the cross-talk of two types of
592 receptors. *J Biol Chem* 272:23130-23137.
- 593 Wallenius K, Thalen P, Bjorkman JA, Johannesson P, Wiseman J, Bottcher G, Fjellstrom O, Oakes ND (2017)
594 Involvement of the metabolic sensor GPR81 in cardiovascular control. *JCI insight* 2.
- 595 Wang M, Ramos BP, Paspalas CD, Shu Y, Simen A, Duque A, Vijayraghavan S, Brennan A, Dudley A, Nou E,
596 Mazer JA, McCormick DA, Arnsten AF (2007) Alpha2A-adrenoceptors strengthen working memory networks
597 by inhibiting cAMP-HCN channel signaling in prefrontal cortex. *Cell* 129:397-410.
- 598 Werry TD, Wilkinson GF, Willars GB (2003) Mechanisms of cross-talk between G-protein-coupled receptors
599 resulting in enhanced release of intracellular Ca²⁺. *Biochem J* 374:281-296.

600 Yang J, Ruchti E, Petit JM, Jourdain P, Grenningloh G, Allaman I, Magistretti PJ (2014) Lactate promotes
601 plasticity gene expression by potentiating NMDA signaling in neurons. *Proc Natl Acad Sci USA* 111:12228-
602 12233.

603 Zhang C, Schmidt JT (1999) Adenosine A1 and class II metabotropic glutamate receptors mediate shared
604 presynaptic inhibition of retinotectal transmission. *J Neurophysiol* 82:2947-2955.

605 Zhang Y, Chen K, Sloan SA, Bennett ML, Scholze AR, O'Keefe S, Phatnani HP, Guarnieri P, Caneda C, Ruderisch
606 N, Deng S, Liddelow SA, Zhang C, Daneman R, Maniatis T, Barres BA, Wu JQ (2014) An RNA-sequencing
607 transcriptome and splicing database of glia, neurons, and vascular cells of the cerebral cortex. *J Neurosci*
608 34:11929-11947.

609

610

611 **Figure legends**

612 **Figure 1. HCAR1 expression in primary mouse neurons.** (a) HCAR1 mRNA expression level in primary neurons
613 (n=4 experiments). HCAR1 mRNA transcript levels were normalized relative to that of the housekeeping gene
614 GAPDH. (b) Representative PCR image of HCAR1 gene expression in WT versus HCAR1 KO animals. WT and
615 HCAR1 KO embryonic tissue were obtained from animals used to originate neuronal primary cultures. A WT
616 band at 470pb and a HCAR1 KO band at 800bp can be observed. (c) Representative confocal images of primary
617 cortical neurons immunostained for NeuN (green) and mRFP-HCAR1 (red), along with Hoechst nuclear staining
618 (blue) and the overlay image. (d) Quantification of mRFP, NeuN and mRFP-NeuN positive cells shown as the
619 percentage of Hoechst positive cells (n=5 experiments, repeated 3 times per experiment). Scale bar 40µm.

620

621 **Figure 2. HCAR1 activation decreases mEPSC frequency and modulates intrinsic membrane properties of**
622 **mouse cortical neurons.** (a) Representative mEPSCs traces from a neuron recorded in the presence and in the
623 absence of 3CI-HBA 40µM for WT and HCAR1 KO. Voltage-clamp recordings of mEPSCs were performed in the
624 presence of TTX (1µM) and bicuculline (60µM) with neurons clamped at -70mV. (b) Summary of mEPSC
625 frequency and amplitude (percent of baseline) in response to 3CI-HBA application in WT (n=7) and HCAR1 KO
626 neurons (n=6). A depression of mEPSC frequency, but not amplitude, was observed upon HCAR1 activation in
627 neurons prepared from WT but not from HCAR1 KO mice. (c) Representative superimposed averaged traces of
628 1000 events from the same WT neuron in the absence (full line) and in the presence of 3CI-HBA (dotted line),
629 and table showing corresponding average kinetic values of all events from WT and KO in the presence and in
630 the absence of 3CI-HBA, demonstrating similar kinetics in WT and KO neurons. Significance is shown in
631 comparison to baseline and among conditions. (d) *Left:* Representative responses to paired pulses protocols
632 using an interstimulus interval of 50ms in WT neurons before and after HCAR1 activation (*left*). Arrows
633 represent the stimulation. *Right:* Summary graph of PPR results (n=7). Significance is shown between the
634 control condition and after 3CI-HBA application. (e) Representative traces from neurons recorded before and

635 after HCAR1 activation (*left*), obtained from a series of current injections (0 to 450pA, 1 sec, 50pA increments);
636 the response to 150pA current injection is shown. Summary graph (*right*) of the effect of HCAR1 activation on
637 neuronal firing frequency following steps of current injection (n=5). The firing frequency (Hz) was calculated
638 from the number of AP evoked by 150pA current injection. Significance is shown between the control and 3Cl-
639 HBA conditions.

640

641 **Figure 3. Effect of neuronal activation in neuronal calcium spiking activity.** (a) Representative traces of
642 calcium spiking in control or 5mM L-lactate containing solutions, for both WT and HCAR1 KO neurons. (b) The
643 effect of the HCAR1 agonist 3Cl-HBA on spontaneous calcium activity of neurons was concentration
644 dependent, with an IC₅₀ value of 21.5±6.1µM (n=177 neurons from 23 experiments). The IC₅₀ value was
645 obtained by non-linear curve fitting using Levenberg-Marquardt algorithm. (c) Effect of HCAR1 activation on
646 calcium spiking frequency from wild-type and HCAR1 KO neurons with 5mM L-lactate (WT: n=66 cells, 16 exp.;
647 HCAR1 KO: n= 81 cells, 16 exp.), 1mM 3,5-DHBA (WT: n=57, 16 exp.; HCAR1 KO: n=74 cells, 12 exp.) or 40µM
648 3Cl-HBA (WT: n=31 cells, 3 exp.; HCAR1 KO : n=32 cells, 5 exp.). Spiking frequency is shown as percentage of
649 activity measured in control condition. The effect of HCAR1 activation was reversible in all experiments (*not*
650 *shown*). Significance is shown in comparison to control and among conditions. (d) Comparison of basal
651 spontaneous spiking frequencies of neurons from WT (n=16) and HCAR1 KO (n=16).

652

653

654 **Figure 4. Adenylyl cyclase, cAMP, and PKA involvement in neuronal HCAR1 signaling.** (a) Activation of AC
655 with Forskolin (10 µM) increased spiking activity in both WT (n=44 cells, 5 exp.) and HCAR1 KO (n=29 cells, 3
656 exp.) neurons compared to their respective baseline activity. Application of 3,5-DHBA (1mM), in sequence with
657 Forskolin, decreased spiking activity in WT, but not in HCAR1 KO neurons (b). Inhibition of AC with SQ22536
658 (10 µM) decreased spiking activity in WT neurons (n= 46 cells, 6 exp.). Application of 3,5-DHBA, in sequence

659 with SQ22536, did no further decrease neuronal activity. (c) Representative trace of the effects of HCAR1
660 activation on cAMP levels measured using the Epac2-camps FRET sensor. The FRET (CFP/YFP) ratio,
661 proportional to the cAMP levels, is shown for a single neuron along time. Application of the AC activator
662 forskolin (10 μ M) caused a rapid signal rise, and the subsequent HCAR1 activation using 3Cl-HBA (40 μ M)
663 reversed this increase. (d) Summary of absolute FRET ratio values in the presence of forskolin before and after
664 stimulation of HCAR1 using 3Cl-HBA. The graph shows individual values plotted along with the mean value of
665 all experiments (n=6 cells, 6 exp.). (e) Inhibition of PKA with H-89 (1 μ M) decreased spiking activity in WT
666 neurons (n=64 cells, 6 exp.). Application of 3,5-DHBA, in sequence with H-89, did not further decrease
667 neuronal activity. Significance is shown in comparison to control and among conditions in panels (a), (b) and
668 (e).

669

670

671 **Figure 5. HCAR1 interaction with other G_i-coupled receptors for the modulation of neuronal activity.** (a)
672 HCAR1 was first activated using 3,5-DHBA (1mM) and in a second phase, the agonist of A1R, CPA (30nM) was
673 co-applied, which caused a stronger decrease in spiking activity compared to HCAR1 activation alone. The
674 same protocol was performed with a reverse order of receptor activation, *i.e.* first CPA and then 3,5-DHBA
675 application. Whereas the secondary 3,5-DHBA application caused a partial reversal of inhibition in neurons
676 from WT animals (b), it had no effect on neurons from HCAR1 KO animals (c). The effect of the co-activation of
677 A1R with HCAR1 in the presence of gallein (10 μ M), a $\beta\gamma$ subunit signaling inhibitor (d), or U73122 (10 μ M), a
678 PLC blocker (e) is shown. Both treatments prevented the partial reversal of inhibition observed in (b). (f) Effect
679 of $\beta\gamma$ subunit inhibition using gallein (10 μ M) and (g) of PLC blockade with U73122 (10 μ M) on HCAR1 activation
680 alone using 3Cl-HBA-HBA (40 μ M). Inhibition of $\beta\gamma$ subunit partially reverted HCAR1 effect on neural activity,
681 however PLC blockade did not influence HCAR1 effect. Data are means \pm SEM from (a) 21 cells, 4 exp., (b) 20

682 cells, 4 exp., (c) 27 cells, 4 exp. , (d) 26 cells, 4 exp., (e) 14 cells, 3 exp., (f) 33 cells, 4 exp., (g) 22 cells, 3exp.

683 Significance is shown in comparison to control and among conditions.

684

685 **Figure 6. HCAR1 modulation of neuronal activity.** Scheme depicting the modulatory effect brought about by

686 HCAR1, when activated in isolation (**a**) or with concurrent activation of other G_i-coupled GPCRs (**b, c**).

687 **Table 1. Anti-HCAR1 primary antibody specificity**

688

Anti-HCAR1 primary antibody (Source, Reference)	Epitope	IHC		WB	
		WT	HCAR1 KO	WT	HCAR1 KO
Santa Cruz, SC-32647	C-terminal, extracellular domain of human HCAR1	§	§	+	+
Santa Cruz, SC-32648	C-terminal, cytoplasmic domain of human HCAR1	+	+	-	-
Sigma, SAB1300090	Mouse GPR81-S296, aa 276-329	+	+	+	+
Sigma, SAB1300793	Rat GPR81-R320, aa 286-332	+	+	§	§
Sigma, SAB1300089	Human GPR81-296, aa 310-353	+	+	+	+
Sigma, SAB1300792	Mouse GPR81-R203, aa 193-230	+	+	§	§
Sigma, SAB1300791	Mouse GPR81-C7, aa 7-36	+	+	-	-
Novus Biologicals, NLS2095	19 aa peptide from C-terminus of human HCAR1	+	+	§	§
Novus Biologicals, NBP1-51956	C-QQLARQARMKKATR (internal region)	+	+	§	§

Experiments were performed in brain slices of cortex, hippocampus and cerebellum. (+) represents positive signal/band and (-) represents negative/absence of signal/band; IHC, immunohistochemistry; WB, Western blot; §, not tested; aa, amino acid. See **Table 1-1** and **Table 1-2**.

689 **Table 2. Summary of behavioral phenotype of WT versus HCAR 1 KO** ^a

690

		WT	n	HCAR1 KO	n
(1)	Weight (g)	26.3 ± 0.4	12	27.4 ± 0.9 ^{ns}	12
	Food consumption (g)	3.5 ± 0.3	10	3.3 ± 0.2 ^{ns}	10
	Water consumption (ml)	3.1 ± 0.2	10	3.7 ± 0.3 ^{ns}	10
	Total travel distance (cm)	55374 ± 7352	10	52059 ± 5197 ^{ns}	10
	Dark phase	41985 ± 5419		43263 ± 4515 ^{ns}	
	Light phase	13389 ± 2885		8796 ± 2224 ^{ns}	10
	Total time in the nest (min)	46136 ± 3363	10	47686 ± 3442 ^{ns}	10
	Dark phase	21681 ± 1781		20962 ± 2537 ^{ns}	
	Light phase	24454 ± 1785		26724 ± 1369 ^{ns}	
(2)	Rearing (number/min)	8.6 ± 0.7	12	9.8 ± 0.5 ^{ns}	12
	Number of Grooming (number/min)	0.6 ± 0.1	12	0.6 ± 0.1 ^{ns}	12
	Grooming duration (sec)	24 ± 5.3	12	25 ± 5.5 ^{ns}	12

691

^aExperiments were performed on independent animals. (1) Phenotypic cage observations. (2) Free observations. Data are shown as means ± SEM, *ns*, not significant Student unpaired t-test.

692

693 **Table 3.** Effect of HCAR1 activation on passive properties of cortical cultured neurons ^a

	Control	3CI-HBA 40 μ M
RMP (mV)	-59.3 \pm 1.1	-62.9 \pm 1.3*
R _N (M Ω)	97.3 \pm 6.4	77.5 \pm 6.2*
Rheobase (pA)	78.6 \pm 6.8	93.6 \pm 8.7*
Time constant (ms)	16.4 \pm 1.1	18.8 \pm 0.5*

^a Experiments were performed in 5 independent WT neurons. All parameters were tested in all cells used for analysis. Data are shown as means \pm SEM, *p<0.05 Student paired t-test. RMP: resting membrane potential; R_N: input resistance.

694

Table 4. HCAR1 interactions with GABA_B and α_{2A} receptors and neuronal activity ^a

	WT		HCAR1 KO	
<u>GABA_BR / HCAR1</u>	Freq. (%)	<i>n</i> _{cells} , <i>n</i> _{exp}	Freq. (%)	<i>n</i> _{cells} , <i>n</i> _{exp}
3,5-DHBA ^b	32.3±6.9	37, 4	--	
→ + Baclofen	2.6±3.3 *			
Baclofen	13.9±0.8	12, 3	53.2±3.4	35, 4
→ + 3,5-DHBA	43.6±5.5 *		51.7±4.5 ^{ns}	
<u>α_{2A}R / HCAR1</u>				
3,5-DHBA	48.4±8.9	44, 4	--	
→ + Guanfacine	8.4±3.3 *			
Guanfacine	24.2±2.8	36, 4	26.8±8.4	29, 4
→ + 3,5-DHBA	54.2±4.1 *		27.2±8.2 ^{ns}	

^a Data are expressed as percent of the frequency observed in baseline conditions. Data are shown as means ± SEM, *p<0.05, *ns*, not significant ANOVA, Bonferroni correction, for *n* cells from *n* experiments. Statistical significance indicated for comparisons between the two displayed conditions. ^b Concentrations used: 1mM 3,5-DHBA, 0.5μM baclofen and 10μM guanfacine.

695 **Table 5. Lack of functional interactions among A1, GABA_B, and α_{2A} receptors ^a**

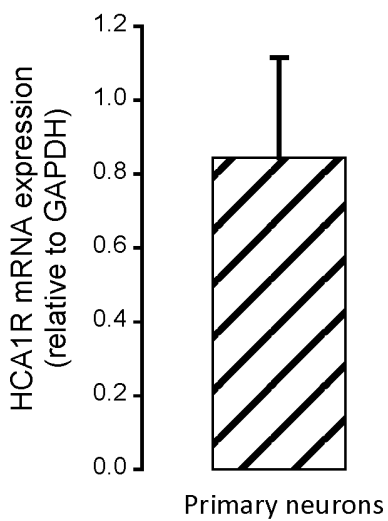
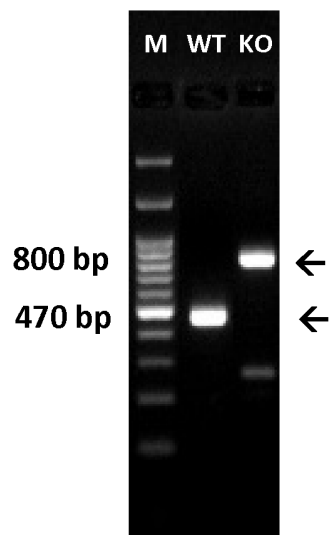
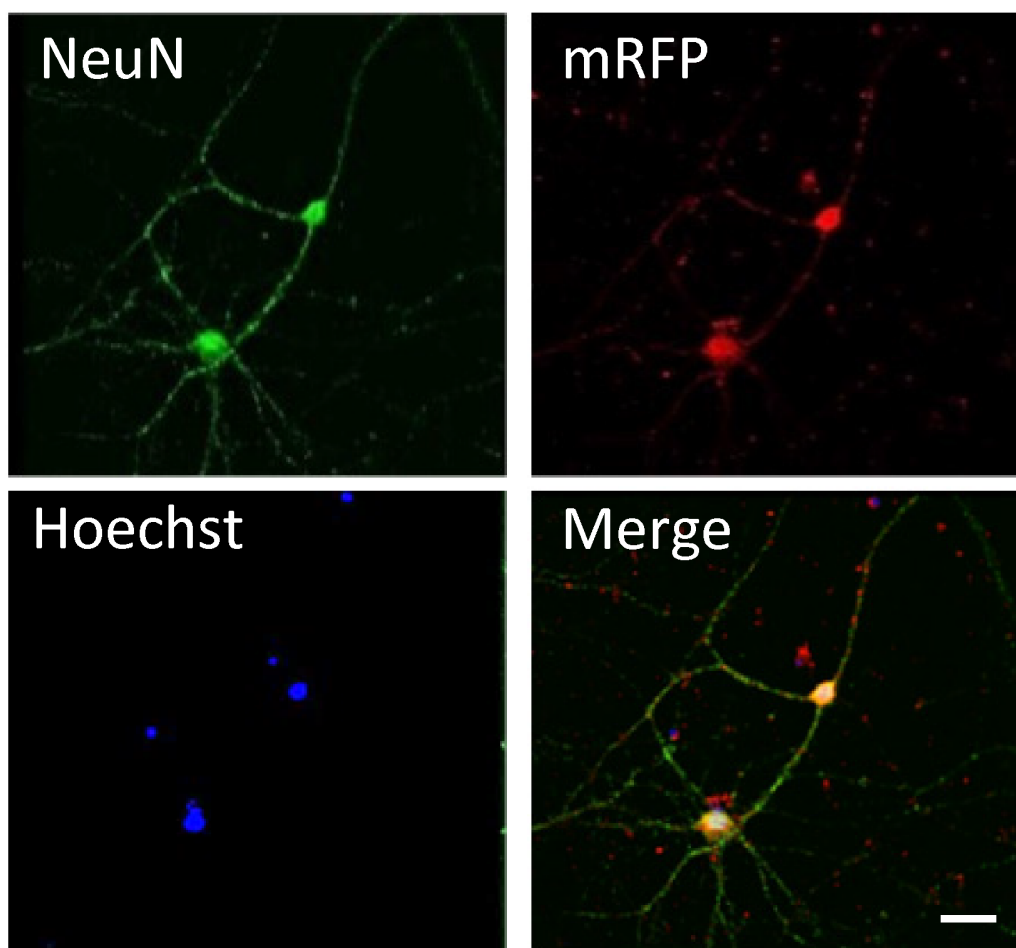
<u>A1R / GABA_BR</u>	Freq. (%)	<i>n</i> _{cells} , <i>n</i> _{exp}
CPA ^b	2.4±2.1	20,3
→ + Baclofen	1.8±1.6 ^{ns}	
Baclofen	41.5±7.6	18,3
→ + CPA	2.7±0.2 *	
<u>A1R / α_{2A}R</u>		
CPA	8.9±8.8	19,3
→ + Guanfacine	8.4±3.3 ^{ns}	
Guanfacine	39.2±8.3	17,3
→ + CPA	3.8±1.9 *	
<u>α_{2A}R / GABA_BR</u>		
Guanfacine	51.2±11.6	16,3
→ + Baclofen	42.4±9.8 ^{ns}	
Baclofen	60.1±5.4	18,3
→ + Guanfacine	41.6±7.5 ^{ns}	

^a Data are expressed as percent of the frequency observed in baseline conditions. Data are shown as means ± SEM, *p<0.05, *ns*, not significant ANOVA, Bonferroni correction, for *n* cells from *n* experiments. Statistical significance indicated for comparisons between the two displayed conditions. ^b Concentrations used: 30nM CPA, 0.5μM baclofen, 10μM guanfacine.

696 **Table 6. Mechanism of HCAR1 interaction with GABA_B and α_{2A} receptors^a**

<u>GABA_BR / HCAR1</u>	Freq. (%)	<i>n</i> _{cells} , <i>n</i> _{exp}
Baclofen ^b	41.5±7.6	13,3
→ + 3,5-DHBA + Gallein	41.3±6.96 ^{ns}	
<hr/>		
Baclofen	36.6±16.2	19,3
→ + 3,5-DHBA + U73122	12.5±2.4 ^{ns}	
<hr/>		
<u>α_{2A}R / HCAR1</u>		
Guanfacine	40.5±6.0	22,4
→ + 3,5-DHBA + Gallein	46.0±6.3 ^{ns}	
<hr/>		
Guanfacine	51.2±11.7	17,3
→ + 3,5-DHBA + U73122	47.5±9.5 ^{ns}	
<hr/>		

^a Data are expressed as percent of the frequency observed in baseline conditions. Data are shown as means ± SEM, *ns*, not significant ANOVA, Bonferroni correction, for *n* cells from *n* experiments. Statistical significance indicated for comparisons between the two displayed conditions. ^b Concentrations used: 1mM 3,5-DHBA, 0.5µM baclofen, 10µM guanfacine, 10µM gallein, 10µM U73122.

a**b****c****d**